Vector-tracking-based GNSS/INS Deep Coupling and Experiment Platform for Urban Scenarios

Yan, Zhe

IEEE
2021

Yan , Z , Ruotsalainen , L , Gao , N & Chen , X 2021 , Vector-tracking-based GNSS/INS Deep Coupling and Experiment Platform for Urban Scenarios . in 2021 International Conference on Sensing, Measurement & Data Analytics in the era of Artificial Intelligence (ICSMD) . IEEE , International Conference on Sensing, Measurement & Data Analytics in the era of Artificial Intelligence , Nanjing , China , 21/10/2021 . https://doi.org/10.1109/ICSMD53520.2021

http://hdl.handle.net/10138/341252
https://doi.org/10.1109/ICSMD53520.2021.9670857

acceptedVersion

Vector-tracking-based GNSS/INS Deep Coupling and Experiment Platform for Urban Scenarios

2021 International Conference on Sensing, Measurement & Data Analytics in the era of Artificial Intelligence (ICSMD) | 978-1-6654-2747-0/21/$31.00 ©2021 IEEE | DOI: 10.1109/ICSMD53520.2021.9670857

Zhe Yan
Southeast University
Nanjing, China.
Department of Computer Science
University of Helsinki
Helsinki, Finland
seuyanzhe@163.com

Laura Ruotsalainen
Department of Computer Science
University of Helsinki
Helsinki, Finland
laura.ruotsalainen@helsinki.fi

Ning Gao
School of Instrument Science and Engineering
Southeast University
Nanjing, China
ninggaoseu@163.com

Xiyuan Chen*
School of Instrument Science and Engineering
Southeast University
Nanjing, China
chxiyuan@seu.edu.cn

***Abstract*—Vector-tracking-based GNSS/INS deep coupling is a promising method for high-precision and robust navigation in urban challenging environments, especially for weak and dense multipath scenarios. However, the research on this topic is far from enough due to the complexity of multipath interference and system structure. Herein, a typical vector delay/frequency-locked loop is introduced. Then, based on this vector tracking loop, two different deep coupled schemes are proposed according to different approaches to estimating the corrections for the inertial navigation system. At last, the experiment based on a vehicular field collection and a software-defined platform was designed in which all the commonly used stand-alone-receiver-based and GNSS/INS-based methods are tested and compared. The results preliminarily illustrate the effectiveness and superiority of the deep coupling methods designed, on positioning and measurement improvement, especially in a weak signal and multipath scenario.**

Keywords—GNSS/INS, deep coupling, multipath, urban scenarios

I. INTRODUCTION

In urban canyon scenarios, high-precision vehicular positioning and navigation system using the Global Navigation Satellite System (GNSS) is challenged by many complex elements affecting the measurement quality, which seriously affects the positioning accuracy. These challenges are caused by e.g. signal occlusion, multipath, non-line-of-sight (NLOS) error, environment noise, and platform vibration. Among them, the undesirable multipath error remains a dominant source of errors and is still a popular topic among the academic and engineering community [1].

The integration of GNSS and inertial navigation system (INS) is a common method and widely used in vehicular positioning. However, the measurement from GNSS receiver is still sensitive to multipath propagation and not getting improved in a loosely or a tightly integrated GNSS/INS system [2], which sometimes leads to the failure of the integration filter. Vector tracking [3][4] and vector-tracking-based GNSS/INS deep coupling [2][5] have the innate advantages in overcoming multipath impacts because the tracking channels are dependent of one another. Compared with the loosely and tightly integrated GNSS/INS systems which provide INS with corrections only, deep coupling constructs a joint tracking loop aided by INS and navigation filter. This innovation can improve the performance of tracking and system robustness in challenging environments, for example, a dense multipath environment in an urban area. Using the high-precision estimations from INS or navigation filter, tracking loop is limited to a small margin of multipath error so that the GNSS measurement and loop robustness can be improved. However, when a low-cost MEMS-INS (Micro-Electro-Mechanical System, MEMS) is used, the performance tends to degrade dramatically.

This advanced benefit has been widely verified by many researchers. Ren and Petovello used the vector tracking and INS-assisted tracking to improve the maximum-likelihood bit decoding so that a high-sensitive GNSS receiver for weak signals can be achieved [6]. The vector tracking for dynamic weak signals in urban environments was designed as well by [7]. An adaptive GPS vector tracking loop with the detection and isolation of the contaminated channels was designed in [8] for poor signal quality but not specifically for multipath environments. The performance enhancement of the vector tracking in signal blocking situations was observed in [9]. The NLOS signal was detected by probabilistic approach and estimated by an augmented-state Kalman filter on the basis of vector tracking according to Jiang's work [10]. However, aiming at urban scenarios, the multipath propagation is not well addressed in the literatures. Hsu evaluated the performance of the vector delay-locked loop (VDLL) with multipath and NLOS reception, and the results of positioning and code discriminator were presented [11]. A GPS/GLONASS vector tracking receiver was designed and tested in an unknown multipath environment in [12]. But there are few literatures reported on the deep coupling system for multipath signals.

As a result, the performance and mechanism of the vector tracking and vector-tracking-based GNSS/INS deep coupling method in dense multipath scenarios needs further exploration. To achieve this, the vector tracking and deep coupling schemes will be firstly provided. Then, for the convenience of future study and contrastive analysis, an experiment platform will be implemented on the basis of a software-defined receiver, including scalar tracking, EKF based scalar tracking, vector delay/frequency-locked loop (VDFLL), loose integration, tight integration, and deep coupling. In experiment part, this platform will be tested using both multipath-free and multipath data. Eventually, we will draw the conclusions.

*Xiyuan Chen is the corresponding author. (e-mail: chxiyuan@seu.edu.cn).

II. Vector Tracking Loops

A. Description of Vector Tracking

The main purpose of the tracking loops is to estimate the Doppler frequency f_d, initial carrier-phase φ and code-delay τ of the received signal accurately and dynamically, then replicate a local satellite signal. Accordingly, vector frequency-locked loop (VFLL), vector phase-locked loop (VPLL), and vector delay-locked loop (VDLL) are proposed respectively. The concept of vector tracking is put forward firstly on the basis of VDLL. And to determine the position and velocity of a vehicle, the VDLL and VFLL are widely used, while the VPLL is suitable for the high-precision positioning technologies where carrier phase measurements are essential. So the VPLL is not considered in the following implementation.

Due to the inter-channel aiding information, the tracking of a contaminated channel can be assisted by other clean channels. For example, when a channel is polluted by multipath receptions, the multipath error contained in the position solution is smaller than that in the pseudo-range measurement of this polluted channel, no matter whether this channel is used in positioning or not. So the feedback can be constructed using line-of-sight vector to assist the channel in tracking the direct reception. If the change in position obtained from INS can be used, the multipath error in position solution is expected to be further narrowed, and so is the line-of-sight feedback. This is the innate benefit of vector tracking and the vector-based deep coupling. The spatial coupling of different channels is based on the fact that they share the same position solution.

B. Design of VDFLL

A typical VDFLL is the combination of VDLL and VFLL and can be seen in Fig. 1 where the blue blocks are the inherent part in a conventional receiver while the green ones the new part of VDFLL.

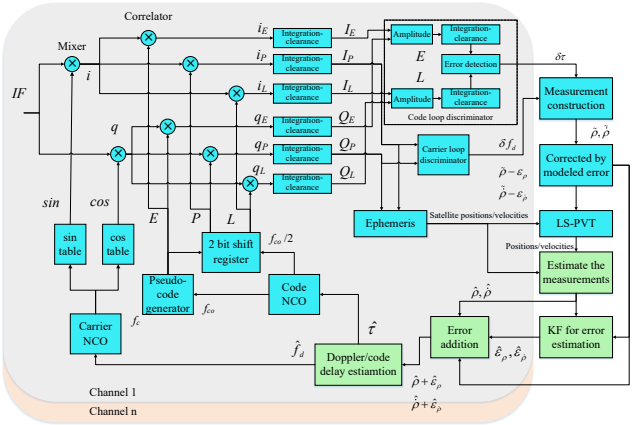

Fig. 1. Strucure of a typical VDFLL

After obtaining the errors of code delay and Doppler frequency, the raw measurements can be calculated, namely pseudo-range $\tilde{\rho}$ and pseudo-range rate $\tilde{\dot{\rho}}$. ε_ρ denotes all the error corrections that can be modeled of the pseudo-range, including the clock error provided by ephemeris, tropospheric error, and ionospheric error, etc. And $\varepsilon_{\dot{\rho}}$ denotes the modeled error correction of pseudo-range rate, for example, the clock drift's error. Then, the position, velocity, and time (PVT) will be computed using the least-squares method. In addition, the PVT computation can use a Kalman filter option as well.

According to the user's position and velocity from PVT block, we can simply obtain an estimated pseudo-range $\hat{\rho}$ and pseudo-range rate $\hat{\dot{\rho}}$ if the satellite's position and velocity have been computed using ephemeris. It needs to be noted that the estimated pseudo-range and pseudo-range rate along the line-of-sight vector are so ideal that are quite different from the received signal. However, the main task of the tracking is trying to keep the locally replicated signal exactly the same with the received one. Otherwise, though the estimated pseudo-range is the ideal true value, there will still be a large error in the discriminator output so will the measurement of the next epoch. So it is important to add all the errors back on the estimated pseudo-range $\hat{\rho}$ and pseudo-range rate $\hat{\dot{\rho}}$ before calculating the estimated code delay $\hat{\tau}$ and Doppler $\hat{f}_d$. Because not all the errors on raw measurements can be or will be modeled precisely, for example, the thermal noise, multipath error, NLOS error, and so on, it is necessary to estimate the errors $\hat{\varepsilon}_\rho$ and $\hat{\varepsilon}_{\dot{\rho}}$ that need to be added on the estimated measurement. In our implementation, only the clock error provided by ephemeris and tropospheric error are modeled and used for correction before PVT.

To estimate $\hat{\varepsilon}_\rho$ and $\hat{\varepsilon}_{\dot{\rho}}$, a Kalman filter is designed with the state vector expressed as below

$$\mathbf{X}_k = [\delta x, \delta y, \delta z, \delta \dot{x}, \delta \dot{y}, \delta \dot{z}, \delta t_b, \delta t_d]^T, \tag{1}$$

where the state variables are the position and velocity errors in ECEF coordinate system, clock bias error in meter, and clock drift error in meter per second. Suppose the time update period is T and the discretized state equation can be given by

$$\mathbf{X}_{k+1} = \mathbf{\Phi}_k \mathbf{X}_k + \mathbf{\Gamma}_k \mathbf{W}_k, \tag{2}$$

where the transfer matrix $\mathbf{\Phi}_k$ can be detailed as

$$\mathbf{\Phi}_k = \begin{bmatrix} \mathbf{I}_{3\times3} & T\cdot\mathbf{I}_{3\times3} & \mathbf{0}_{3\times2} \\ \mathbf{0}_{3\times3} & \mathbf{I}_{3\times3} & \mathbf{0}_{3\times2} \\ \mathbf{0}_{2\times3} & \mathbf{0}_{2\times3} & \mathbf{C}_{2\times2} \end{bmatrix}, \ \mathbf{C}_{2\times2} = \begin{bmatrix} 1 & T \\ 0 & 1 \end{bmatrix}. \tag{3}$$

Because the error in PVT can be projected onto the line-of-sight vector, we can relate the PVT error with the error of pseudo-range as

$$\delta\rho_j = \mathbf{A}_j \cdot \boldsymbol{\delta}\mathbf{P} + \delta t_b - \varepsilon_\rho, \tag{4}$$

where $\boldsymbol{\delta}\mathbf{P} = [\delta x, \delta y, \delta z]^T$, and $\mathbf{A}_j$ is the unit line-of-sight vector from user receiver to the jth satellite and can be expressed as

$$\mathbf{A}_j = \left[-\frac{x_u - x_{sj}}{r_j}, -\frac{y_u - y_{sj}}{r_j}, -\frac{z_u - z_{sj}}{r_j} \right], \tag{5}$$

where (x_u, y_u, z_u) and (x_{sj}, y_{sj}, z_{sj}) are the positions of user receiver and the *j*th satellite respectively. r_j is the Euclidean distance between (x_u, y_u, z_u) and (x_{sj}, y_{sj}, z_{sj}).

In a similar way, we can relate the PVT error with the error of pseudo-range rate as

$$\delta\dot{\rho}_j = \mathbf{A}_j \cdot \boldsymbol{\delta}\mathbf{V} + \delta t_d - \varepsilon_{\dot{\rho}}. \tag{6}$$

Suppose n channels or n visible satellites will be used, the measurement equation can be given by

$$\mathbf{Z}_k = \mathbf{H}_k \mathbf{X}_k + \mathbf{V}_k, \tag{7}$$

where the measurement is

$$\mathbf{Z}_k = [\tilde{\rho}_k^1 - \hat{\rho}_k^1, \cdots, \tilde{\rho}_k^n - \hat{\rho}_k^n, \tilde{\dot{\rho}}_k^1 - \hat{\dot{\rho}}_k^1, \cdots, \tilde{\dot{\rho}}_k^n - \hat{\dot{\rho}}_k^n]_{2n\times 1}^T, \tag{8}$$

and the measurement matrix $\mathbf{H}_k$ can be given by

$$\mathbf{H}_k = \begin{bmatrix} a_{x,k}^1 & a_{y,k}^1 & a_{z,k}^1 & 0 & 0 & 0 & 1 & 0 \\ \vdots & \vdots & \vdots & \vdots & \vdots & \vdots & \vdots & \vdots \\ a_{x,k}^n & a_{y,k}^n & a_{z,k}^n & 0 & 0 & 0 & 1 & 0 \\ 0 & 0 & 0 & a_{x,k}^1 & a_{y,k}^1 & a_{z,k}^1 & 0 & 1 \\ \vdots & \vdots & \vdots & \vdots & \vdots & \vdots & \vdots & \vdots \\ 0 & 0 & 0 & a_{x,k}^n & a_{y,k}^n & a_{z,k}^n & 0 & 1 \end{bmatrix}_{2n\times 8}. \tag{9}$$

In equation (9), $\mathbf{A}_k^n = \left[a_{x,k}^n, a_{y,k}^n, a_{z,k}^n\right]$ is the line-of-sight vector defined by equation (5).

The carrier and code numerically-controlled oscillators (NCOs) in this vector tracking loop will be adjusted by the control values computed using the results from the Kalman filter. The control value for the code NCO of the *j*th channel can be described as

$$\hat{\tau}_{k+1}^j = \hat{\rho}_k^j - \tilde{\rho}_k^j + \hat{\varepsilon}_\rho^j + t_{b,k}. \tag{10}$$

In a similar way, the control value for carrier NCO can be given by

$$\hat{f}_{d,k+1}^j = \hat{\dot{\rho}}_k^j - \tilde{\dot{\rho}}_k^j + \hat{\varepsilon}_{\dot{\rho}}^j + t_{d,k}. \tag{11}$$

After this update, the state of the Kalman filter needs to be reset to zero. Then, the whole vector tracking loop is completed.

III. Deep Coupling Structures

A. Description of Deep coupling

The structures of the vector-tracking-based GNSS/INS deeply coupled systems are diverse. This variety and different implementations have been studied and summarized in our previous work, see [5]. Herein, based on the VDFLL we introduced above, the deep coupling is preliminarily constructed by simply using the position/velocity information from INS to estimate measurements instead of using the results from LS-PVT, as shown in Fig. 2.

However, as is well known, the INS needs to be corrected continuously, otherwise the error will keep growing with time. According to the different methods used to estimate the error of INS, two different deep coupling structures will be introduced as follows.

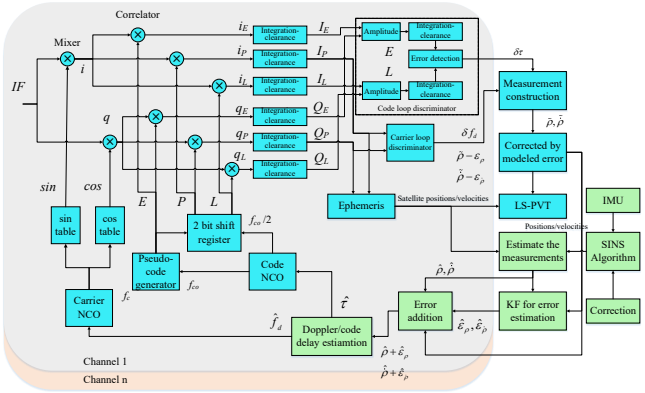

Fig. 2. Strucure of a typical deep coupling system

B. Deep coupling structure 1

For the purpose of autonomous integrity monitoring, the conventional PVT resolution is usually reserved even though in a deep coupling system. This presents a good opportunity to estimate the INS correction in a loose integration way. The error state is composed of 15 variables given by position errors in latitude, longitude, and height $[\delta L, \delta\lambda, \delta h]^T$, velocity errors in east, north, and up $[\delta v_E, \delta v_N, \delta v_U]^T$, attitude errors $[\varphi_x, \varphi_y, \varphi_z]^T$, accelerometer bias errors $[\nabla_x, \nabla_y, \nabla_z]^T$, and gyroscope bias errors $[\varepsilon_{bx}, \varepsilon_{by}, \varepsilon_{bz}]^T$. The measurement equation can be given by

$$\mathbf{Z}_{k,loose} = \mathbf{H}_{k,loose}\mathbf{X}_{k,loose} + \mathbf{V}_{k,loose}, \tag{12}$$

where the measurements are the position/velocity differences between INS and GNSS, namely

$$\mathbf{Z}_{k,loose} = [\mathbf{P}_k^{INS} - \mathbf{P}_k^{GNSS}, \mathbf{V}_k^{INS} - \mathbf{V}_k^{GNSS}]. \tag{13}$$

The measurement matrix $\mathbf{H}_{k,loose}$ is

$$\mathbf{H}_{k,loose} = \begin{bmatrix} \mathbf{I}_{3\times 3} & \mathbf{0}_{3\times 3} & \mathbf{0}_{3\times 9} \\ \mathbf{0}_{3\times 3} & \mathbf{I}_{3\times 3} & \mathbf{0}_{3\times 9} \end{bmatrix}. \tag{14}$$

In this deep coupling method, the Kalman filter shares the same structure with the GNSS/INS loose integration system but is more robust because of the vector tracking.

C. Deep coupling structure 2

To estimate the INS correction, tight integration can be used as well which is generally expected to be more robust than the loose one. For the tight integration, apart from the 15 state variables in the loosely integrated system, two extra parameters are included, the errors of clock bias and clock drift represented by δt_b and δt_d respectively. The measurements are the differences between the pseudo-range/rate estimated by INS and the ones measured by GNSS as below

$$\mathbf{Z}_{k,tight} = [\rho^j_{k,INS} - \rho^j_{k,GNSS}, \dot{\rho}^j_{k,INS} - \dot{\rho}^j_{k,GNSS}]^T_{2n\times 1}. \quad (15)$$

The measurement matrix $\mathbf{H}_{k,tight}$ is similar with equation (9) but the corresponding elements for attitude errors, accelerometer bias error, and gyroscope bias errors are all zeros. In addition, the pseudo-range/rate are computed in ECEF coordinate system, so the position error and velocity error need to be transformed from ECEF to Geographic and Navigation coordinate systems respectively. The corresponding transform matrices can be respectively given by

$$\mathbf{C}^e_c = \begin{bmatrix} -(R+h)\sin L\cos\lambda & -(R+h)\cos L\sin\lambda & \cos L\cos\lambda \\ -(R+h)\sin L\sin\lambda & (R+h)\cos L\cos\lambda & \cos L\sin\lambda \\ [R(1-e^2)+h]\cos L & 0 & \sin L \end{bmatrix} \quad (16)$$

$$\mathbf{C}^e_t = \begin{bmatrix} -\sin\lambda & -\sin L\cos\lambda & \cos L\cos\lambda \\ \cos\lambda & -\sin L\sin\lambda & \cos L\sin\lambda \\ 0 & \cos L & \sin L \end{bmatrix}. \quad (17)$$

This integration filter and the Kalman filter in Fig. 2 can be merged into one filter. But the loop and tight integration may have different update frequencies, so we decided to keep them both in our implementation.

IV. Experiment and Discussion

A. Experiment Platform Description

To verify the effectiveness and superiority of the VDFLL and the two deep coupling structures introduced above, experiments using a soft-ware defined platform were designed. In this experiment, 7 different methods are implemented, including scalar tracking, EKF scalar tracking, VDFLL, loose integration, tight integration, and two deep coupling schemes, as shown in Fig. 3. Among them, the description of scalar tracking and EKF tracking can be found in our previous work [4].

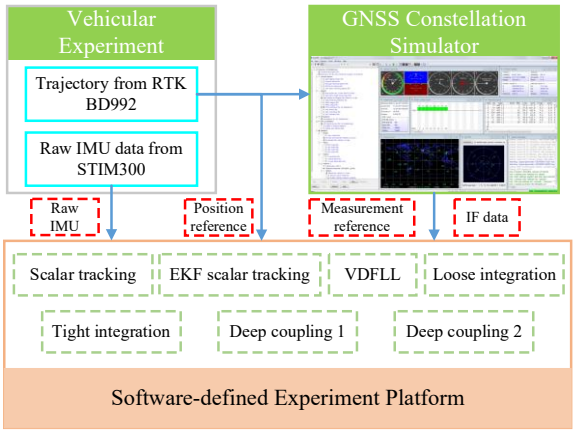

Fig. 3. Experiment platform and flow chart

1) The data was collected through a vehicular experiment conducted in Sipailou Campus, Southeast University, Nanjing, China. Two Trimble BD992 receivers were used as RTK's base station and mobile station respectively with a better precision than 0.01 *m* in horizontal and 0.02 *m* in vertical direction for fixed RTK solution. With a 2 *m* baseline between the position and vector antennas for the mobile receiver, a heading better than 0.1 ° can be acquired.

2) A SPAN-IGM™ system from NovAtel, including a OEM615 GPS L1/L2 receiver and a STIM 300 IMU, was used to collect the raw IMU data with the time stamps from GPS. STIM 300 is a MEMS IMU with a bias instability of 0.3 $°/h$ and an angular random walk of 0.15 $°/\sqrt{h}$ for the gyroscopes, and a bias instability of 0.04 *mg* and a velocity random walk of 0.07 $m/s/\sqrt{h}$ for the accelerometers, according to the Allan variance. The raw IMU output was set to 100 Hz and 2-subsample SINS algorithm was used in our experiments.

Fig. 4. The trajectory in Southeast University for reference.

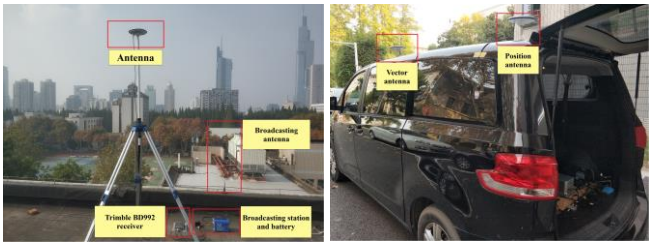

Fig. 5. RTK base station (left) and vehicular experiment (right).

3) As shown in Fig. 4 and Fig. 5, the RTK base station was set on the roof of Central Building. The trajectory begins on GPST 2130 week, 148396 *s* (UTC 17:12:58, November 2nd, 2020) and is 320 *s* long.

4) The trajectory collected by RTK was sent to a GNSS constellation simulator and two different intermediate-frequency (IF) datasets were simulated. One is multipath free and the other is simulated in a weak signal scenario with multipath interference. Besides, the measurement reference can be obtained from the simulator as well. All the experiment results are compared on 10 Hz, both navigation outputs and the reference truth.

B. Multipath Free Trajectory

Using the multipath free dataset, the effectiveness of the methods introduced in this work were tested. The positioning errors in latitude and height are described in Fig. 6 and Fig. 7 respectively where the better accuracy of VDFLL and deep coupling is illustrated well.

As shown in Fig. 7, there are biases in the height of vector tracking, tight integration, and deep coupling. One of the reasons is that the raw relative pseudo-range measurement used contains all the errors uncorrected even the discriminator error, while only the clock error from ephemeris and coarse tropospheric error are added on the estimated pseudo-range from INS. As we have discussed in Section Ⅱ.

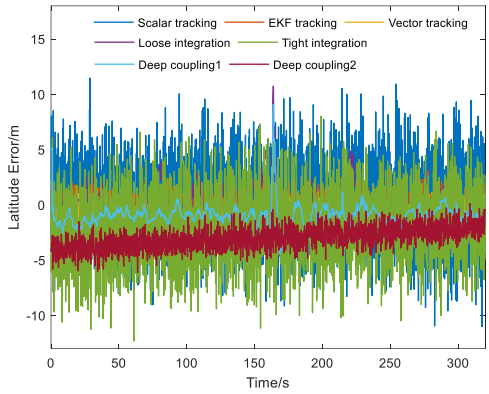

Fig. 6. Positioning errors in latitude of the multipath free dataset.

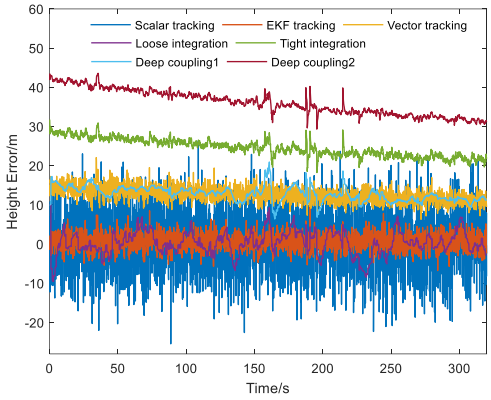

Fig. 7. Positioning errors in height of the multipath free dataset.

TABLE I. STANDARD DEVIATIONS OF THE POSITION ERRORS FOR MULTIPATH FREE TRAJECTORY

Methods	Standard deviations (m), 10Hz		
	Latitude	*Longitude*	*Height*
Scalar tracking	3.39	3.83	7.65
EKF tracking	0.84	0.97	1.98
VDLL+VFLL	0.77	0.82	1.85
Loose integration	1.69	1.45	2.98
Tight integration	3.04	2.62	2.26
Deep coupling 1	0.98	0.67	1.85
Deep coupling 2	0.96	0.97	3.21

The other reason is that the INS is initialized by the positioning result at the moment of filtering start. But the height information from the GNSS receiver fluctuates significantly, which may introduce an initial bias to the INS. Fortunately, this bias can be easily corrected by the LS-PVT block and the standard deviations of the position errors are more important for evaluation. The standard deviations are summarized in Table Ⅰ.

C. Multipath Trajectory

To verify the effectiveness of the methods in multipath scenarios, an IF signal with multipath interference was simulated and some preliminary results were obtained. In this part, only 0-70 *s* trajectory was used for testing and the settings of the constellation simulator are listed in Table Ⅱ.

TABLE II. MULTIPATH SETTINGS FOR THE GNSS SIMULATOR

PRN	Multipath Settings		
	Code delay/chips	*Power attenuation /dB*	*Carrier phase/rad*
6	0.4	-3	0
11	0.6	-3	0
16	0.8	-3	0

Besides, the original power of the signal was set as -130 dB during 0-30 *s* and -132 dB during 30-70 *s*. The positioning errors in latitude and height are described in Fig. 8 and Fig. 9.

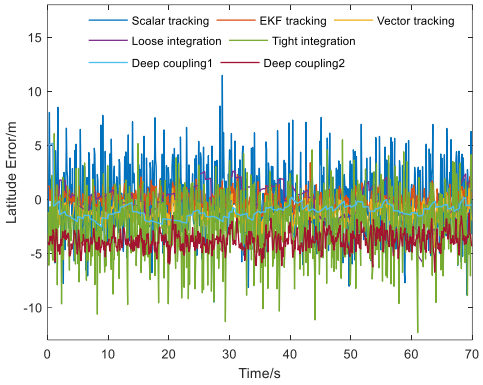

Fig. 8. Positioning errors in latitude of the multipath dataset.

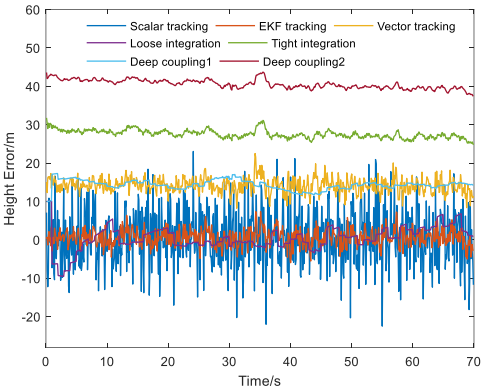

Fig. 9. Positioning errors in height of the multipath dataset.

The similar biases can be observed in this multipath trajectory and the explanation can be also applied here. The standard deviations of the position errors during 0-30 *s* and 30-70 *s* are summarized in Table Ⅲ and Table Ⅳ.

TABLE III. STANDARD DEVIATIONS OF THE POSITION ERRORS FOR MULTIPATH TRAJECTORY 1

Methods	0-30s Standard deviations (m), 10Hz		
	Latitude	*Longitude*	*Height*
Scalar tracking	3.27	3.51	7.15
EKF tracking	0.74	0.88	1.96
VDLL+VFLL	0.70	0.79	1.52
Loose integration	1.22	1.59	3.65
Tight integration	3.10	2.53	0.83
Deep coupling 1	1.23	0.67	1.30
Deep coupling 2	0.71	0.71	0.68

TABLE IV. STANDARD DEVIATIONS OF THE POSITION ERRORS FOR MULTIPATH TRAJECTORY 2

Methods	30-70s Standard deviations (m), 10Hz		
	Latitude	*Longitude*	*Height*
Scalar tracking	3.22	3.39	7.70
EKF tracking	0.87	1.07	2.29
VDLL+VFLL	0.93	1.08	2.21
Loose integration	1.92	1.25	2.28
Tight integration	3.03	2.57	0.96
Deep coupling 1	0.41	0.52	1.06
Deep coupling 2	0.91	0.93	0.95

Since the main influence of multipath is the discriminator bias and larger oscillation which is covered by the larger raw pseudo-range noise, there is no evident influence on the positioning results by the multipath settings herein. But the lower signal power has an obviously adverse impact which makes a bigger positioning error. In general, vector tracking and deep coupling have a better performance in positioning but they are all sensitive to the PVT solution.

However, positioning performance is not the main advantage of vector tracking and deep coupling but the loop robustness. So the pseudo-range measurement errors of PRN 11 for both multipath free and multipath trajectories are drawn in Fig. 10.

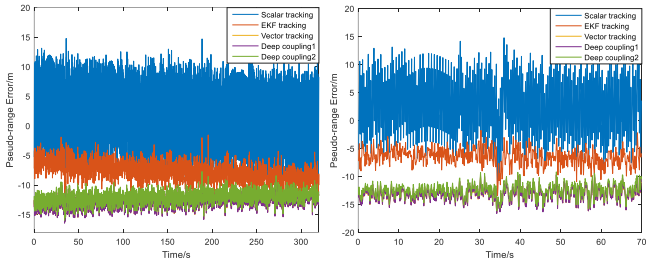

Fig. 10. Pseudo-range measurement error of PRN 11 for multipath free trajectory (left) and multipath trajectory (right).

TABLE V. STANDARD DEVIATIONS OF THE PSEUDO-RANGE ERRORS OF PRN 11

Methods	Multipath free	Multipath	
	0-70s (m)	*0-30s (m)*	*30-70s (m)*
Scalar tracking	5.43	5.39	5.52
EKF tracking	1.45	1.20	1.65
VDLL+VFLL	1.02	0.92	1.30
Deep coupling 1	1.05	0.95	1.34
Deep coupling 2	1.04	0.94	1.32

The standard deviations of the pseudo-range errors of PRN 11 for both multipath free and multipath trajectories are summarized in Table Ⅴ where the better performance on improving measurement and tracking robustness can be observed.

V. CONCLUSION

On the basis of VDFLL tracking loop, two deep coupling structures were introduced herein. To verify the effectiveness of the methods and for the convenience of contrastive analysis, an experiment platform based on a software-defined GNSS receiver was implemented. By vehicular experiment and constellation simulator, the validity of the methods has been proved and the performance improvement in weak signal and multipath environments has been preliminarily demonstrated. Limited by the space, more detailed experiments and analysis will be conducted in the future.

ACKNOWLEDGMENT

This work has been partly funded by the National Natural Science Foundation of China under Grant 61873064, the Academy of Finland, and China Scholarship Council.

REFERENCES

[1] M. Z. Bhuiyan, and E. S. Lohan, “Advanced multipath mitigation techniques for satellite-based positioning applications,” *International Journal of Navigation & Observation*, vol. 2010, pp. 1-16, December 2010.

[2] S. Alban, D. M. Akos, S. M. Rock. “Performance analysis and architectures for INS-aided GPS tracking loops,” Proceedings of the 2003 National Technical Meeting of The Institute of Navigation, Anaheim, USA, January, 2003, pp. 611-622.

[3] M. Lashley, D. M. Bevly and J. Y. Hung, "Performance analysis of vector tracking algorithms for weak GPS signals in high dynamics," *IEEE Journal of Selected Topics in Signal Processing*, vol. 3, no. 4, pp. 661-673, August 2009.

[4] Z. Yan, X. Chen, X. Tang and X. Zhu, “The Implementation and Comparison Between Kalman Filter-based and Vector Tracking Loops,” 2020 International Conference on Sensing, Measurement & Data Analytics in the era of Artificial Intelligence (ICSMD), Xi'an, China, October 2020, pp. 45-50.

[5] Z. Yan, X. Chen, X. Tang, “A novel linear model based on code approximation for GNSS/INS ultra-tight integration system,” *Sensors* vol. 20, no. 11, pp. 1-20, June 2020.

[6] T. Ren and M. G. Petovello, “A stand-alone approach for high-sensitivity GNSS receivers in signal-challenged environment,” *IEEE Transactions on Aerospace and Electronic Systems*, vol. 53, no. 5, pp. 2438-2448, October 2017.

[7] J. Liu, X. Cui, M. Lu and Z. Feng, “Vector tracking loops in GNSS receivers for dynamic weak signals,” *Journal of Systems Engineering and Electronics*, vol. 24, no. 3, pp. 349-364, June 2013.

[8] Z. Sun, X. Wang, S. Feng, et al, “Design of an adaptive GPS vector tracking loop with the detection and isolation of contaminated channels,” *GPS Solutions*, vol. 21, pp. 701–713, April 2017.

[9] A. Tabatabaei, Z. Koohi, M. R. Mosavi, et al, “Intelligent vectorised architecture for performance enhancement of GNSS receivers in signal blocking situations,” *Survey Review*, November 2020.

[10] C. Jiang, B. Xu, and L. T. Hsu, “Probabilistic approach to detect and correct GNSS NLOS signals using an augmented state vector in the extended Kalman filter,” *GPS Solution*, vol. 25, no. 72, March 2021.

[11] L. T. Hsu, S. Jan, P.D. Groves, et al, “Multipath mitigation and NLOS detection using vector tracking in urban environments,” *GPS Solutions*, vol. 19, pp. 249–262, April 2015.

[12] A. Tabatabaei, M. R. Mosavi, H. S. Shahhoseini, et al, “Vectorized and federated software receivers combining GLONASS and GPS,” *GPS Solutions*, vol. 21, pp. 1331–1339, July 2017.